Thermal kinetic and mechanical behaviors of pressure-assisted Cu nanoparticles sintering A molecular dynamics study

Hu, Dong; Cui, Zhen; Fan, Jiajie; Fan, Xuejun; Zhang, Guoqi

DOI
10.1016/j.rinp.2020.103486

Publication date
2020

Document Version
Final published version

Published in
Results in Physics

Results in Physics 19 (2020) 103486

Contents lists available at ScienceDirect

Results in Physics

journal homepage: www.elsevier.com/locate/rinp

Thermal kinetic and mechanical behaviors of pressure-assisted Cu nanoparticles sintering: A molecular dynamics study

Dong Hu [a,1], Zhen Cui [a,1], Jiajie Fan [a,b], Xuejun Fan [c], Guoqi Zhang [a,*]

[a] Department of Microelectronics, Delft University of Technology, 2628 CD Delft, the Netherlands
[b] Center for Shanghai Silicon Carbide Power Devices Engineering & Technology Research, Academy for Engineering & Technology, Fudan University, Shanghai 200433, China
[c] Department of Mechanical Engineering, P.O. Box 10028, Lamar University, Beaumont, TX 77710, USA

ARTICLE INFO

Keywords:
Cu nanoparticle
Pressure-assisted sintering
Molecular dynamics simulation
Mechanical property

ABSTRACT

A molecular dynamics (MD) simulation was performed on the coalescence kinetics and mechanical behavior of the pressure-assisted Cu nanoparticles (NPs) sintering at low temperature. To investigate the effects of sintering pressure and temperature on the coalescence of the nanoparticles, sintering simulations of two halve Cu NPs were conducted at the pressure of 0–300 MPa and the temperature of 300–500 K. A transition of the dominant coalescence kinetics from slight surface diffusion to intensive grain boundary diffusion and dislocation driven plastic flows were found when pressure was applied. Furthermore, atomic trajectories showed the effect of temperature on sintering was strongly dependent on the microstructures of Cu NPs. The atomic diffusion around defects can be significantly promoted by the elevated temperature. Additionally, based on the sintered structures, uniaxial tension simulation was implemented with a constant strain rate. Stress–strain curves and evolution of dislocation activities were derived. Improved mechanical behaviors, including larger elastic modulus and larger tensile strength, were obtained in the structure sintered under higher pressure and temperature. Among this study, sintering temperature and pressure consistently exhibited the same relative impact on affecting both coalescence and the mechanical properties of the sintered structure.

Introduction

The wide bandgap (WBG) semiconductors, represented by SiC and GaN, are promising candidates in high-power semiconductor devices because of its great merits of higher power density, larger breakdown voltage, and higher operation temperature, compared to conventional Si devices [1–5]. However, one of the big challenges for the WBG semiconductors-based power devices is the reliability issue of the die-attach layer. As the physical limits of lead-free solder cannot meet the high operating temperature required for next-generation WBG semiconductors power devices, an alternative die-attach material with better thermal dissipation and mechanical behaviors is practically needed [6].

In the past decades, low-temperature sintering of metallic nanoparticles has attracted extensive attention as a promising die-attach technology, because it enables NPs coalescence at a low temperature and sustaining great thermomechanical properties at high temperature. U. Scheuermann *et al.* in the 1990 s first reported the low-temperature sintering of Ag NPs for power electronics packaging, in which the advantages of this technology, e.g., the small variation of thermal conductivity and the less build-in stress, were presented [7]. After that, many works demonstrated that the die-attach layer using sintered NP has better thermal, mechanical, and electrical properties, compared to the common lead-free solder layer [8–11].

Generally, the coalescence of NPs during sintering involves at least five mechanisms for mass transport, including grain boundary diffusion, surface diffusion, volume diffusion, dislocation activity, and surface evaporation–condensation [12]. The contributions of diffusion mechanisms on the evolution of particle's shape were theoretically studied in the works of Coblenz *et al.* [13], Venkateshwarlu *et al.* [14] and Djohari *et al.* [15,16]. By using Frenkel's model based on continuum theory [17,18], those work showed that the atomic concentration gradient and stress gradient contributed the driving forces for the mass transport of NPs from the cent to the surface, resulting in the NPs coalescence. At the atomic scale, molecular dynamic (MD) studies on NPs sintering provided

* Corresponding author.
E-mail address: G.Q.Zhang@tudelft.nl (G. Zhang).
[1] Dong Hu and Zhen Cui equally contribute to present work.

https://doi.org/10.1016/j.rinp.2020.103486
Received 3 August 2020; Received in revised form 16 September 2020; Accepted 6 October 2020
Available online 12 October 2020

an insight in understanding various NPs coalescence (Cu [19,20], Au [21], Fe [22], Ta [23]). Goudeli *et al.* established a two-NP model to investigate the thermodynamic process of Cu NPs sintering [24]. It was found that elevated temperature can lead to a larger degree of NPs coalescence by affecting its atomic diffusion rate as well as the degree of plastic deformation. Except that, Ding *et al.* investigated the effect of the relative crystal orientation on neck growth, in which it was observed that a reorientation of particles took place to match a preferred crystalline orientation at the beginning of the sintering [25]. Additionally, the work done by Grammatikopoulos *et al.* studied the size effect on NPs sintering [26]. It was found that the smaller NPs have more dislocation nucleation, growth, and sliding of stacking faults at the junction of nanoparticles, compared to larger NPs, which efficiently promote the NPs to coalesces into the larger and uniform grains.

The pressure is another significant influential factor on NPs coalescence. From the perspective of experiments, Knoerr and Schletz reported that the density of the sintered layer of Ag NPs can be improved from 58% to 90% when the sintering pressure increased from 0 MPa to 30 MPa [27]. The increased density corresponded to the improvement of electrical and thermal conductivity of the sintered Ag layer. Zhao *et al.* applied pressure-assisted sintering in power electronic packaging, and better reliability performance was obtained compared to those soldered power module [28]. Therefore, the sintering pressure is necessary to ensure excellent reliability of the sintered layer in a harsh environment. Based on the continuum theory, it is believed that the external pressure applied on NPs can be amplified at the neck region, which further causes a large mechanical stress gradient from the mass central to the neck surface, accelerating the atomic immigration towards the neck region.

However, above-mentioned understandings on the underlying relation between external pressure and microstructure evolution during NPs sintering are not clear. In particular, the question of how pressure affects dislocation activity, surface and bulk transport is still open. In the previous studies, to study the effect of pressure on coalescence, a multi-NPs system was usually adopted that pressure can be applied on the simulation box. Srivastava *et al.* applied 15 GPa on many ligands coated Au NPs to figure out the compression behaviours [29]. In addition, Cheng *et al.* applied 0, 0.25 and 2 GPa to reveal the effect of pressure on densification behaviours of many Cu NPs [30]. Furthermore, the relationship between the mechanical properties of the sintered structure and the sintering behavior is also attractive. By assigning an elongation rate of simulation box along one direction, Yang *et al.* implemented tensile testing simulation on pressureless sintered porous Cu structure at a strain rate of 1×10^8 s^{-1} and stress–strain curves were derived [31]. Similarly, Zhang *et al.* investigated the mechanical strength by performing MD tension simulation on a 41-Nickle NPs sintered system with a strain rate of 1×10^9 s^{-1} [32]. But the effect induced by sintering pressure was not investigated. To reveal the role of pressure, efforts also have been conducted in the two-NP model, where the interconnection process between NPs can be more concentrated on. Wang *et al.* qualitatively analyzed the dislocation-stress interaction under compression condition, while the sintering pressure was not quantitatively controlled and the mechanical properties were not evaluated [33]. Furthermore, Zhang *et al.* directly applied certain tensile strains on pressureless sintered NP pair, instead of continuous tension behaviours [32].

In the present study, by using the MD calculation method, we developed a two-hemispherical NPs model to investigate pressure-assisted sintering of Cu NPs at a low temperature. The effect of various pressure magnitudes on Cu NPs sintering was revealed. The sintering dynamics and microstructure evolutions were analyzed, including neck growth, mean-square displacement (MSD) variations, grain boundary development, and dislocation activity. The mechanisms behind the pressure-assisted sintering were discussed. Moreover, on the basics of pressure-assisted sintered Cu NPs, uniaxial tensile tests with a constant strain rate were employed to investigate its mechanical behaviors.

Simulation methodology

In this study, Large-scale Atomic/Molecular Massively Parallel Simulator (LAMMPS) was employed to conduct all the simulations [34]. The classical embedded atom method (EAM) potential developed by Adam *et al.* [35] was applied for describing the interactions between Cu atoms. This potential has been proven to accurately calculate the cohesive energy, lattice parameters, elastic constants, phase diagram and high-temperature properties of Cu NPs [36–39]. Newton's equation of motion was integrated with the Verlet algorithm. The atomic configurations in our study were visualized by a 3D visualization software, OVITO [40].

Normally, the coalescence for Cu NPs at a low temperature (<573 K) mostly occurs at the contacting neck. The region far away from the neck slightly affects the sintering efficiency of Cu NPs. Thus, in the present model as shown in Fig. 1, two hemispherical Cu NPs with an indentor at the top and a basement at the bottom were constructed. In this model, the basement is used to fix the position of the structure and the indentor is used to apply pressure. Based on previous studies, a radius of NP within 1.4 – 3 nm is feasible to reveal the sintering kinetics [26,31–33,41]. Thus, in the present study, the radius of a single Cu NP is selected as 2.5 nm and the length of indentor and basement is 10 nm. The simulation box has 10,048 atoms for both hemispherical Cu NPs and 32,000 atoms in total. In addition, in many published works, 2–5 Å initial distance between NPs were selected. Therefore, in the present study, a 3.6 Å initial distance is selected, that is the length of lattice constant of Cu and located in the acceptable range reported in the literature [42–44].

In all simulations, a timestep of 1 fs was chosen for calculation and the periodic boundary condition was applied in the three dimensions. The positions and velocities of each Cu atoms were recorded in every 1 ps. Fig. 1 exhibits the geometric parameters obtained in the simulation. To obtain the neck size, a dynamically allocated block region with 3.5 Å thickness was empirically defined in the neck region, containing less than three layers of Cu NPs. The neck size at each specific timestep was calculated from the coordinates of boundaries atoms along [010] direction. Furthermore, the MSD of the entire system was calculated to evaluate the degree of coalescence, which can be computed by using the following equation,

$$\mathrm{MSD} = \frac{1}{N}\sum_{i=1}^{N}[r_i(t) - r_i(0)]^2 \quad (1)$$

where N is the number of atoms, $r_i(t)$ and $r_i(0)$ are the position of atom i at time t and 0, respectively.

The sintering simulation can be divided into three periods, as described in Fig. 2 with different colours: (1) we first minimized the energy of the system, the coordinates of the atoms were iteratively adjusted (<1000 iterations) until the change in energy between outer iteration was $< 1 \times 10^{-8}$ or the length of the global force vector was $< 1 \times 10^{-8}$ eV/Å. After that, we relaxed the system at 300 K in the NVE ensemble for 50 ps, (2) then the system was heated up to various target temperatures (300 K, 400 K, 500 K) within 200 ps and relaxed for another 200 ps in the NPT ensemble. (3) After that, external pressure was assigned to the top three layers of the indentor to simulate the pressure-assisted sintering. In this step, four different pressures were selected (0, 100, 200, 300 MPa). Afterwards, the entire model was run for 800 ps in the NVT ensemble to reach its equilibrium state. As a note, in the present study, to distinguish the independent effects of temperature and pressure on Cu NPs sintering, the 2nd step was conducted in NPT ensemble with "zero pressure" to avoid the effect from pressure variation on the simulation box. Similarly, the 3rd step was conducted in the NVT ensemble with constant temperature to avoid the effect of temperature variation.

To evaluate the mechanical properties of the sintered structure, the simulation of tensile testing at room temperature was conducted to

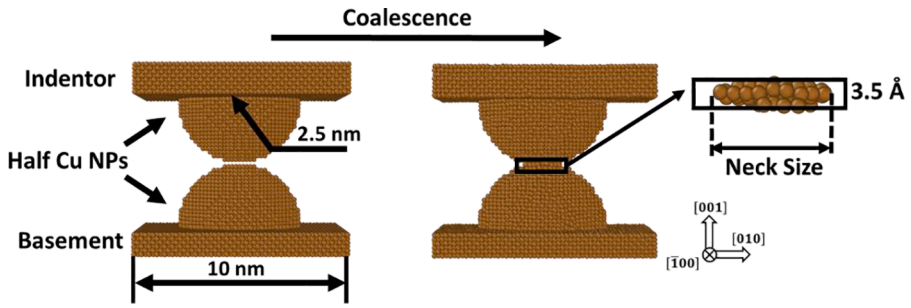

Fig. 1. Two-half Cu NPs model and geometric parameters for the coalescence simulation.

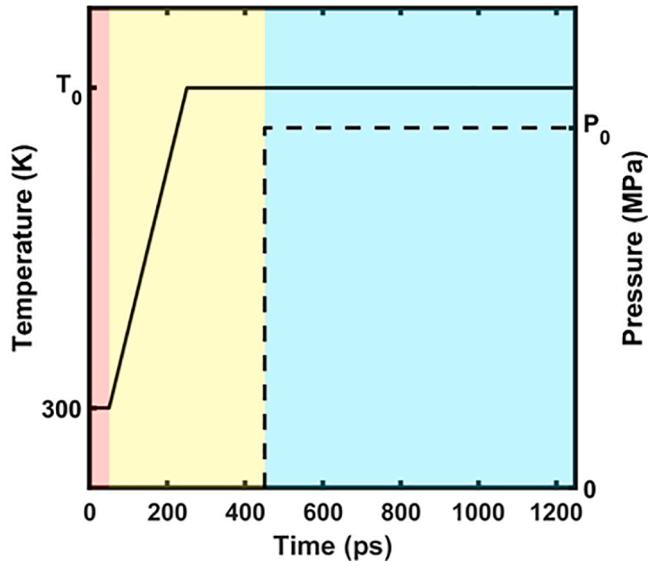

Fig. 2. Illustration for the temperature and pressure profile, in which four different pressures (0, 100, 200, 300 MPa) and three different temperatures (300, 400, 500 K) are selected.

derive the stress–strain curves. Firstly, we removed the pressure applied on indentor and relaxed the entire structure for 500 ps at 300 K in the NVT ensemble, to restore its elastic deformation formed in sintering simulation and obtain an equilibrium state. After that, atoms at the top three layers of the indenter were assigned an upward velocity with a constant strain rate, 7×10^8 s^{-1}, and the average stress for entire sintered Cu NPs was calculate by using following formulation [45]:

$$\sigma_{ab} = -\frac{1}{V}\left[\sum_i m v_a v_b + \frac{1}{2}\sum_i \sum_{n=1}^{N_p} \left(r_{1_a} F_{1_b} + r_{2_a} F_{2_b}\right)\right] \quad (2)$$

where the first term is the kinetic energy contribution to the total stress, m is the mass of atom i, a and b take on values x, y, z to generate the different components. The second term represents the viral contribution due to intra and intermolecular interactions. N_p is the neighbour of atom i, r_1 and r_2 are the positions of the 2 atoms in the pairwise interaction, and F_1 and F_2 are the forces on the 2 atoms resulting from the pairwise interaction. V is the volume of the system to calculate stress, which is equal to the product of atoms number and atomic volume in sintered Cu NPs in the present study. In addition, only a uniaxial tensile loading was applied on structure, thus the zz component was used to derive the stress and the stresses in xx and yy direction were neglected.

Simulation results and discussion

Coalescence kinetic of the pressure-assisted Cu NPs sintering

A whole coalescence process of the pressure-assisted Cu NPs sintering under 300 MPa and 500 K is presented. As Cu is one of typical face-centered cubic (FCC) metals with low stacking fault energy (SFE), the FCC and hexagonal close-packed (HCP) structures can be transformed to each other with thermal or mechanical stimuli such as heating, pressuring, or plastic deformation [46]. Thus, in Fig. 3, the evolution of the total dislocation length and the fraction of HCP ratio are plotted. Data points were recorded every 1 ps. Furthermore, Fig. 4 shows the cross-sections of Cu NPs at several time points, as noted in Fig. 3, where the changes of FCC and HCP structures during sintering are recorded to describe the microstructure evolution. The dislocations and different crystal structures were identified by dislocation analysis (DXA) [47] and common neighbour analysis (CNA) [48].

Based on the information shown in Figs. 3 and 4, the entire sintering dynamics can be divided into three periods. In the first period, we relax the system at 300 K with constant system energy for 50 ps. Two Cu NPs approach to each other, forming a small neck and causing the reduction of the free surface. To prevent the localized higher energy and temperature at the neck region, the velocities on the translational degrees of the atoms are rescaled every 0.01 ps. Then, atoms are further relaxed for energy minimization, forming minor dislocations and HCP crystalline structure. However, with the neck growth, the dislocation and atoms in HCP are gradually vanished, as plotted from 0 to 50 ps in Fig. 3. At 50 ps, a stable structure with neck size, $R = 2.54$ nm, is obtained at the end of the first period, as state $< 2 >$ shown in Fig. 4, in which the FCC lattice is the dominating lattice structure, and no grain boundaries are found at the neck region.

In the second period, the system is heated to 500 K within 200 ps and kept at 500 K for another 200 ps. As the atomic energy increases with the temperature rising, atoms at the neck region rearrange themselves via recrystallization as state $< 3 >$ at 250 ps shown in Fig. 4(a). However, according to Fig. 3, the variations of dislocation and HCP ratio are minor at this stage. Besides, atomic structure transformation from FCC to the amorphous near surface is observed, as the cross-sections of state $< 3 >$ and $< 4 >$ shown in Fig. 4(a). These results indicate that Cu NPs sintering at low temperature mainly via surface diffusion, which results in a slow and slight coalescence.

At the final period, as soon as the 300 MPa pressure is applied at 450 ps, intensive atom arrangements at the neck region start. In a short time, extensive FCC atoms transfer to HCP or amorphous atoms, accompanied by the nucleation of dislocation and formation of stacking faults, as illustrated in state $< 5 >$ to $< 8 >$ in Fig. 4. Meanwhile, the neck size dramatically increases from 2.59 nm to 4.79 nm. Corresponding to such intensive geometry changes, the dislocation length and HCP ratio also experience a rapid increase, as the curves plotted in Fig. 3 from 450 ps to 550 ps. These results indicate that in the post-pressure period, the surface diffusion mechanism loses its dominant role in sintering. Instead, other mechanisms, such as plastic deformation involving dislocation

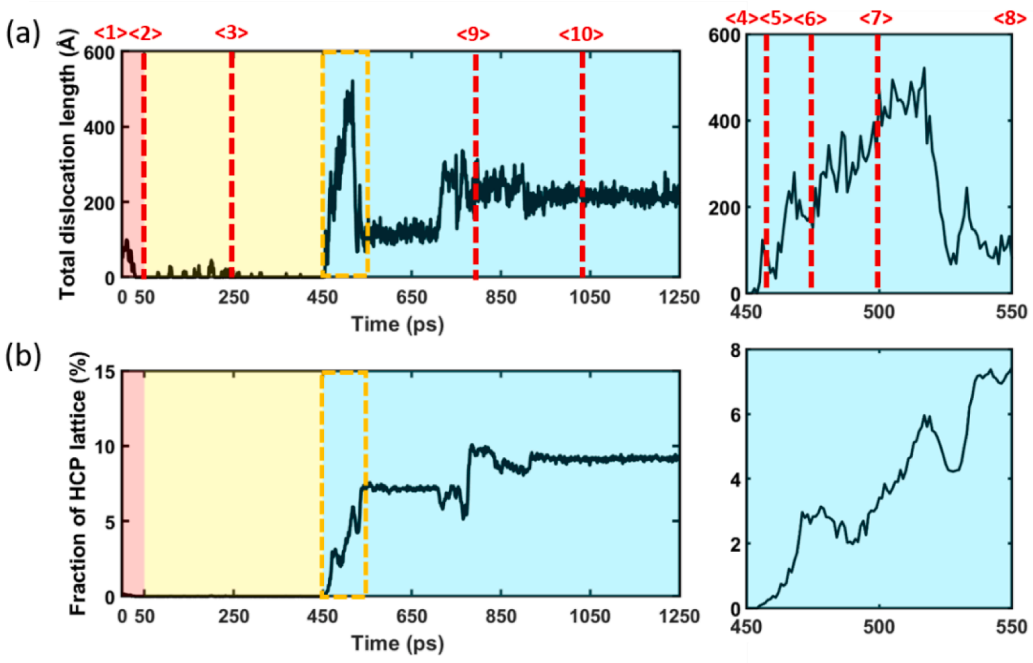

Fig. 3. Crystalline response during the pressure-assisted sintering (a) Evolution of total dislocation length (b) Evolution of HCP ratio.

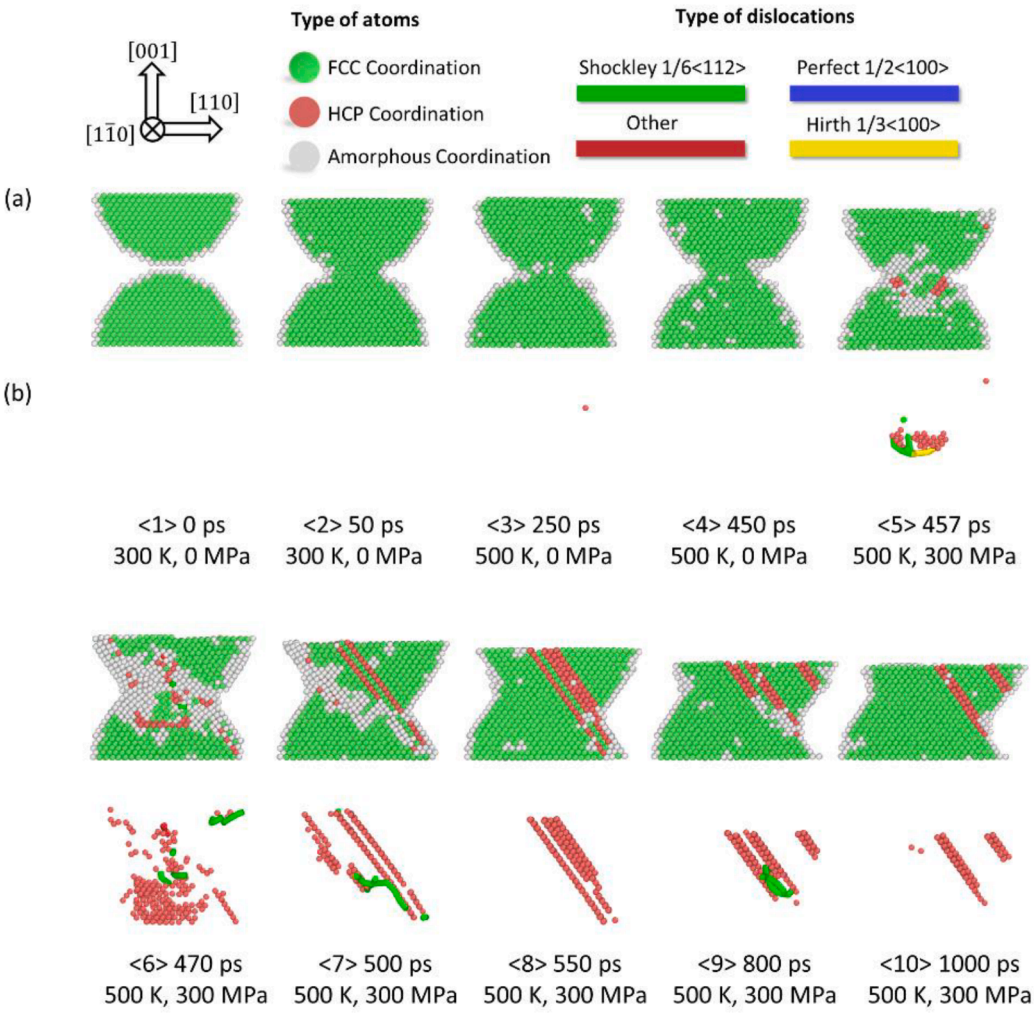

Fig. 4. Snapshots of the cross-section (c) Lattice structures (d) HCP lattice structure and dislocations.

motion and atomic diffusion along grain boundary contribute to the coalescence of Cu NPs. At ~ 750 ps, a slip along {1 1 1} planes occurs, which is responsible for the increases of total dislocation length and HCP lattice ratio in Fig. 3. State < 9 > shown in Fig. 4, as a transition state, confirms this slip by the appearance of Shockley dislocation tangle between two twinning boundaries. During this period, the extensive activated slip systems promote the atom immigration between NPs, resulting in larger neck size. After 900 ps, the growth of neck size and evolution of microstructure gradually slow down as the increased energy induced by pressure is almost released via plastic deformation and mass migration. The slight variation of total dislocation length implies the end of plastic deformation. Finally, twinning boundaries, crossing two hemispherical NPs, are formed as exhibited in state < 10>.

The effect of pressure on the sintering

To further study the effect of pressure on sintering, additional pressure-assisted sintering simulations with three different pressures (0/100/200 MPa) are conducted at 500 K. Evolutions of MSD and neck size are recorded. As plotted in Fig. 4(a) and (b), generally, all cases experience three stages after the pressure is applied on the indentor at 450 ps. Firstly, a dramatic increase in MSD and neck size takes place within a few picoseconds. After that, the coalescence of Cu NPs continually develops, with the steady increases of MSD and neck size of NPs. Consequently, the structures reach the steady-state, in which the structure applied higher pressure shows a better coalescence result. In the case of 300 MPa sintering pressure, it can be seen that the significant increase in Fig. 4 from ~ 700 ps correspond to the dislocation behaviour and lattice transformation shown in Fig. 3. It implies that the dislocation-induced atom rearrangement plays a key role in the coalescence.

To understand the mechanism behind the changing trend induced by pressure, the displacement vectors of Cu NPs sintered under 100 MPa and 300 MPa are plotted in Fig. 6(a) and (b), respectively. The length and direction of the arrow represent the relative distance and the direction of the atom travelled in the past 10 ps. According to Fig. 6(a), the motion of atoms at 462 ps shows that atoms at the upper Cu NPs move downward, and the atoms at bottom vibrate around the original sites. It confirms that the inter-diffusion between the two NPs contributes the quick neck growth. At ~ 500 ps, the motion of atoms becomes weak, leaving the slight atomic diffusion at surface and neck region. However, for the Cu NPs sintering under 300 MPa pressure, a much more extensive atomic motion is observed, as shown in Fig. 6 (b). At 462 ps, atoms at upper NP intensively move downward in the neck region via surface diffusion and volume diffusion. Meanwhile, some atoms at the centre of neck flow to the surface. As a result, an abrupt increase of MSD and neck size is obtained, as the purple line plotted in Fig. 5. At 500 ps, although

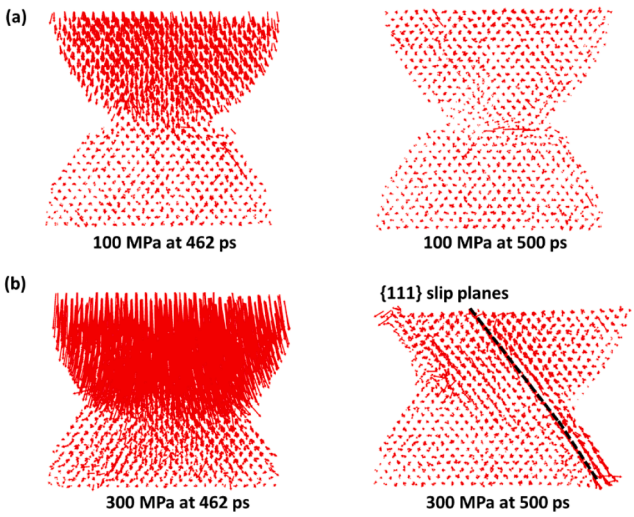

Fig. 6. Displacement vectors of the atoms in the pressure-assisted sintering process under different pressures of (a) 100 MPa; (b) 300 MPa.

the rapid motion of atoms is significantly reduced, atoms around {1 1 1} slip planes are still migrating, continually contributing to the coalescence of Cu NPs. This atomic migration trend is corresponding to the further increasing stage of the purple line in Fig. 5. Finally, Cu NPs under 300 MPa pressure reach the steady-state with a more pronounced coalescence degree, compared to that under 100 MPa pressure.

The difference of atomic motion under 100 MPa and 300 MPa shows that a larger external pressure enables a more intensive plastic flow via inter-migration between Cu NPs, resulting in a faster and stronger necking process. That is the reason why a more abrupt increase in neck size is obtained for the case with a higher pressure. Besides, pressure also affects the defects generation during Cu NPs sintering. As shown in Fig. 4 and Fig. 6(b), extensive defects are created by 300 MPa pressure. As defects play a role as a fast pathway for atomic diffusion, a profound sintering result with large MSD and neck size can be reached thanks to more defects generated during the coalescence. Above comparison shows that the effect of pressure on sintering can be found in two aspects: (1) It induces the plastic deformation during Cu NPs and enhances the atomic diffusion at both surface and volume. (2) Once the applied pressure is large enough, it creates defects and stimulates the microstructure evolutions, increasing the dislocation density, which will, in turn, promote mass transport. As atoms easily move along the high-density dislocations and grain boundaries with low energy, a

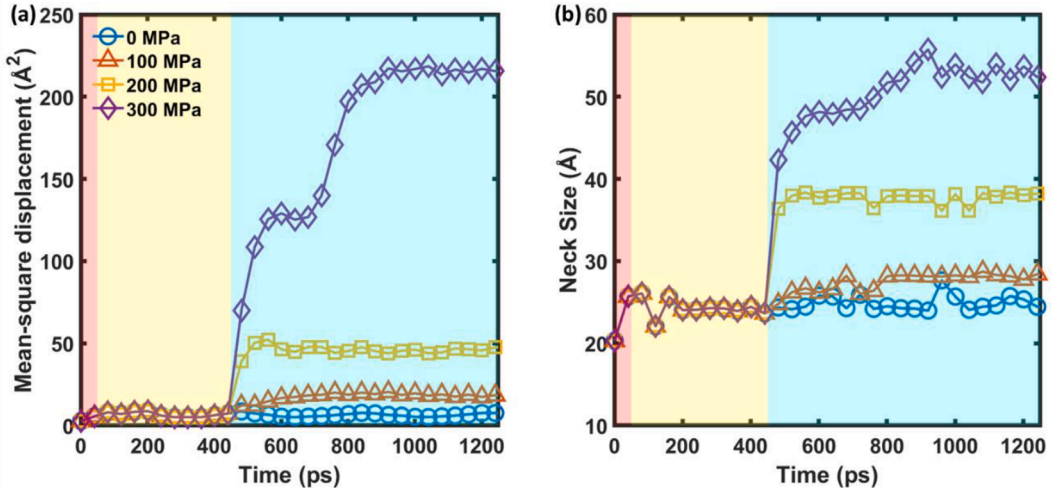

Fig. 5. Dimensional evolutions during press-assisted sintering at 500 K under different pressures (a) MSD (b) Neck size.

successful sintered Cu NPs can be obtained even at a low temperature (<573 K). That is consistent with many experimental works [49–51].

The effect of temperature on the sintering

In pressure-assisted sintering simulation, temperature takes effect on two parts: (1) the independent effect of temperature on sintering in the 2nd step, (2) the coupled effect with pressure on sintering in the 3rd step.

In the 2nd step, with the temperature increases from 300 K to target temperatures, the dimension evolutions of Cu NPs are recorded in Fig. 6. It can be seen that prior to the pressure is applied, the Cu NPs with different temperatures exhibit slight differences in both MSD and neck size. Also, intensive pulsations of neck size are observed at this step. Similar results were also observed in other MD work, in which no evident energy change or neck size increase was observed when the temperature rose from 300 K to 500 K [52].

However, in the 3rd step, once 300 MPa pressure is applied, the rapid changes of NPs dimensions are observed in all cases with different temperatures, as shown in Fig. 7. Afterwards, the coalescence process slows down, both MSD and neck size steady increase before reaching equilibrium. At around 800 ps, the saturated results show that the Cu NPs sintered with higher temperature have the larger MSD and neck size. Comparing to results in the 2nd step, the effect caused by different temperatures with pressure is dramatically amplified. For example, under the pressureless condition, the neck size at 500 K is only 1% larger than that at 300 K. It implies that temperature plays an additional role in NPs sintering when pressure applied on the system.Fig. 8.

To explain the temperature-induced effects, in particular, before and after pressure is applied, the atom trajectory of Cu NPs sintered at 300 K and 500 K are plotted in 8(a) and (b), respectively. In general, both simulations at 300 K and 500 K show a similar magnitude of atomic migration. It can be seen that pressure creates extensive defects and atoms actively migrate around those defects. However, if we compare the trajectory of atoms in detail, the effect of temperature can be discovered. For the Cu NPs sintering under pressure-free condition, the atoms at both temperatures only show a minor surface diffusion at the local region. Therefore, the trajectory of the atoms at 300 K is close to that at 500 K. However, when the external pressure is applied at 500 ps, the different performance of atomic migration shows up. At 300 K, the atoms around {1 1 1} slip planes, intensively migrate and the atoms at surface flow into the neck area. In contrast, at 500 K, a more intensive atomic migration on {1 1 1} slip planes occurs, around which atoms show a trend to move from upper to neck region and surface. Moreover, the surface diffusion at 500 K also shows much visible than that at 300 K. Thus, those comparisons provide us two important information: (1) For the structure with low concentrations of defects, as the structure at 110 ps, the elevated temperature only promotes the atomic diffusion at the surface, that takes a limited effect on Cu NPs coalescence. This is the reason why the slight differences of Cu NPs dimensions are obtained in the 2nd step. (2) However, for the structure with high concentrations of defects, as the atomic migration around defects can be strongly promoted by higher temperature, thus temperature plays a significant role in sintering. Due to more defects are generated by the applied pressure, an amplified effect of temperature in the 3rd step is observed. The higher temperature induces more intensive atomic migration to improve the Cu NPs coalescence.

Tensile testing simulation

The stress–strain curve and evolution of total dislocation length for the Cu NPs sintered at 500 K and 300 MPa are depicted in Fig. 9. It can be seen that the sintered Cu NPs can endure the stress of more than 1.9 GPa at the 4.83% yield strain and fractures at 72.85% strain. To better understand the underlying tensile deformation, the cross-sections of the deformed atomic configurations are extracted in Fig. 10. It can be seen that the spikes of stress correspond to the changing trend of the total dislocation length.

Before the yield strain, the tensile stress almost linearly increases to 1.91 GPa, as the extension of sintered Cu NPs commences with the elastic deformation. The small stress releases before the yield are induced by the extinction of the existing defects, which further causes an FCC dominated structure as shown in state $< 2 >$ in Fig. 10. After the yield strain, the stress is abruptly released, accompanied by the obvious increase of total dislocation length. It indicates the structure steps into the stage of plastic deformation. As state $< 3 >$ shows, twinning boundaries are formed in both Cu NPs and a dislocation tangle is formed near the neck region. From state $< 3 >$ to state $< 5 >$, the neck of Cu NPs continually shrinks with the increasing upper displacement. A serrated evolution of stress was observed. It is because the defects induced by tensile loading actively evolve, from nucleation to propagation to annihilation, causing the instability of microstructures of Cu NPs. Consequently, the tensile stress becomes zero with elongation of $\varepsilon = 72.85\%$, and the total dislocation length almost stays unchanged, representing the end of plastic deformation induced by the tensile test. At this moment, the configuration of state $< 6 >$ shows a tensile fracture with a 45° chisel-edge rupture.

The stress–strain curves for Cu NPs sintered at various temperature and pressure conditions are plotted in Fig. 11(a) and (b). After the first yield point, during the plastic deformation, the variation in the curves become severe. It is because that the sintered structure is complex and

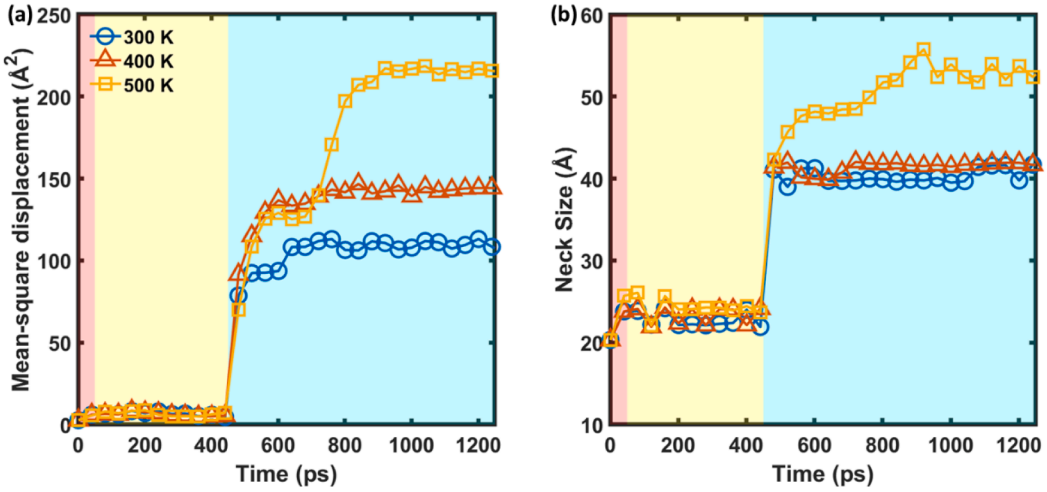

Fig. 7. Dimensional evolutions during 300 MPa pressure-assisted sintering at different temperatures (a) MSD (b) Neck size.

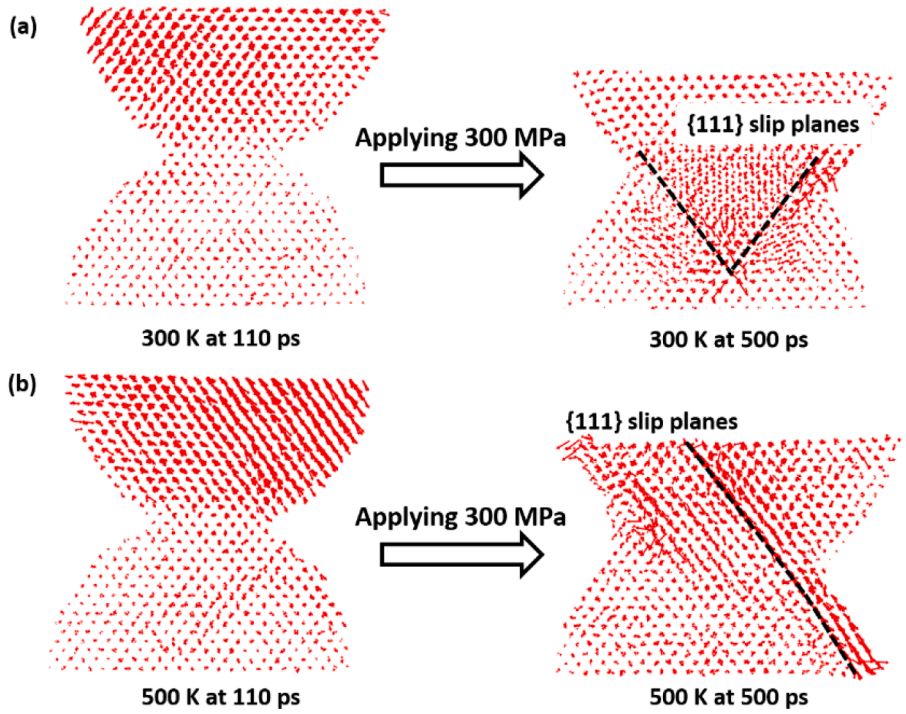

Fig. 8. Displacement vectors of the atoms in the pressure-assisted sintering process at different temperatures of (a) 300 K; (b) 500 K.

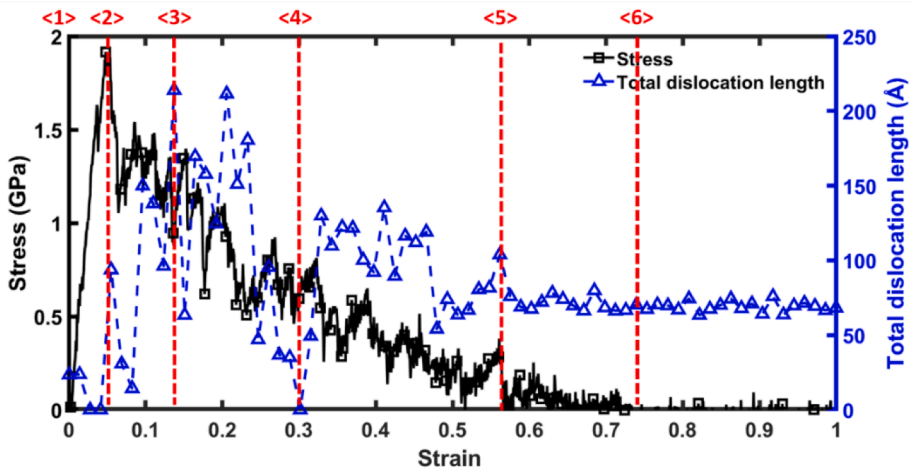

Fig. 9. Stress–strain response and evolution of dislocation length during the tensile deformation.

the area of cross-section dramatically changes accompanying intensive dislocation activities. It can be seen that under the same sintering temperature, the structure sintered with higher pressure results in higher tensile strength and elastic modulus, as well as larger fracture strain. For example, the tensile stress for the structure pressureless-sintered is 1.04 GPa that is much lower than the 1.91 GPa tensile strength for the structure sintered under 300 MPa. It can be concluded that a profound mechanical behavior of Cu NPs can be obtained by increasing its sintering pressure. For the structures sintered under the same pressure but different temperatures, Fig. 11(b) shows that the elevated temperature can also lead to the better mechanical behavior of Cu NPs. But, compared to the effects caused by sintering pressure, the effect of temperature is less significant than the pressure as the increase of tensile strength, from 1.55 GPa to 1.91 GPa, is less than that induced by adding pressure.

Additionally, these findings on mechanical behaviours are consistent with our abovementioned sintering results that the pressure plays a more significant role in Cu NPs coalescence than the role of temperature. As shown in Fig. 5, a higher sintering pressure leads to the larger MSD and neck size of Cu NPs, indicating a better degree of Cu NPs coalescence. The similar trend is also obtained for the Cu NPs sintered with different temperatures, as shown in Fig. 7. For the results obtained in tensile tests, Fig. 12 shows that in general, better elastic modulus and tensile strength are obtained on the structure with a larger neck size. It indicates that better coalesced Cu NPs enable more profound mechanical properties. In a recent experimental study, an increasing tendency of elastic modulus of the sintered Cu NPs with smaller porosity was reported, which means that there exists a positive correlation between the mechanical behavior and the coalescence degree of Cu NPs [53]. The magnitudes of elastic modulus obtained in the experiments vary in the range of 30–80 GPa that is a qualitative agreement to our simulation results. Therefore, the results obtained in the present study may provide a fundamental explanation of some experimental studies about pressure-assisted NPs sintering. In future, based on the present model, the effects

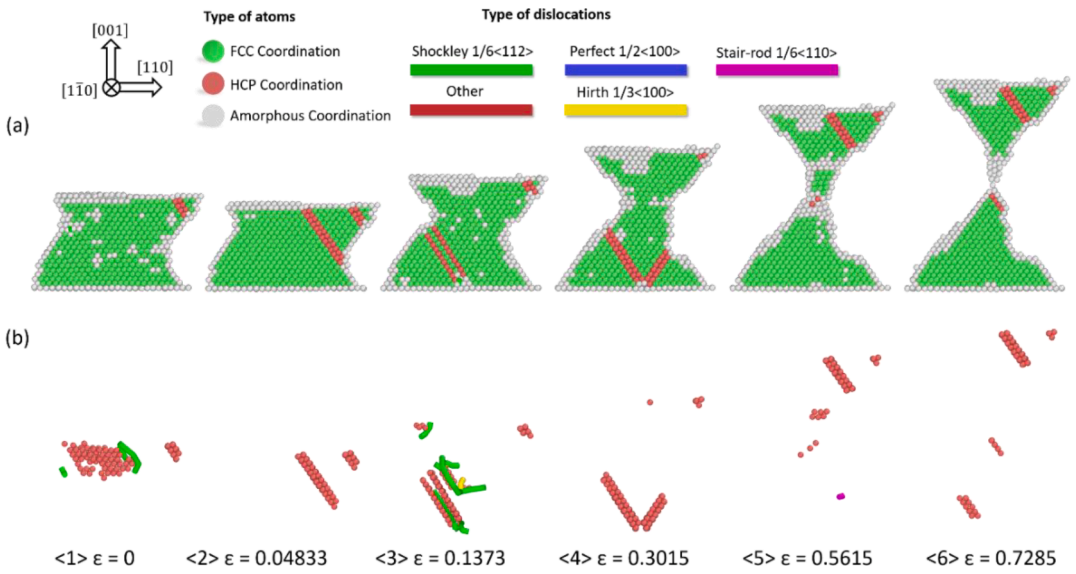

Fig. 10. (a) Snapshots of configurations of lattice structures (b) Snapshots of configurations of HCP lattice structure and dislocations.

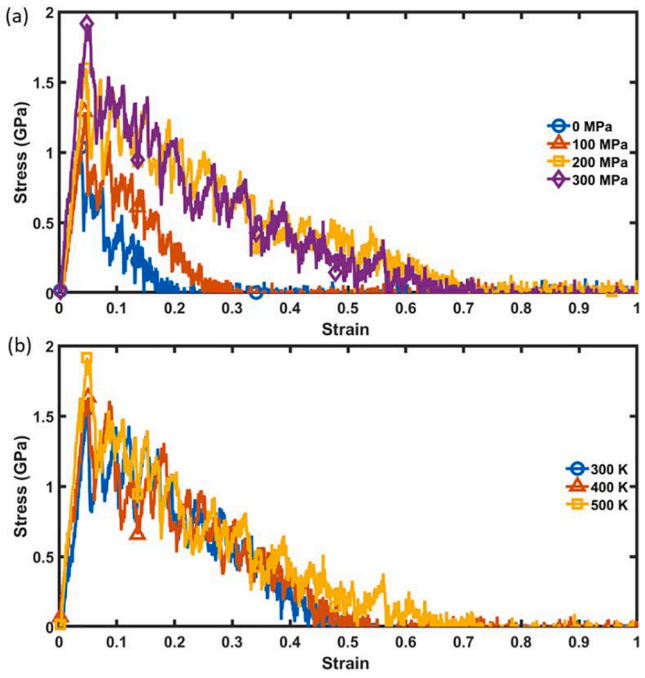

Fig. 11. Tensile stress–strain curve of the system sintered at (a) different pressures (b) different temperatures.

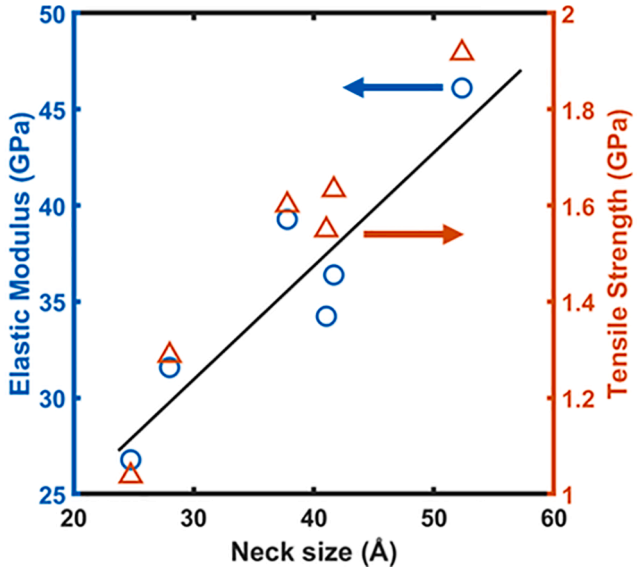

Fig. 12. Elastic modulus and tensile strength of the sintered structure with different neck sizes.

of oxidation and organic coating on Cu NPs will be studied. And, a multiple NPs model, that is closer to reality, will be conducted to compare with our on-going experiments.

Conclusion

In this study, the coalescence kinetics and mechanical properties of pressure-assisted Cu NPs at low temperature were investigated by using MD simulations. The effects of the sintering pressure and temperature on MSD, neck size and the mechanical response of the sintered Cu NPs systems were analyzed. In the pressure-assisted sintering, it was found that the pressure was a more dominant mechanism in sintering more coalesced Cu NPs than the temperature. By applying pressure to the Cu NPs, the transition of the dominant coalescence kinetics could change from slight surface diffusion to the intensive volume diffusion and plastic flow driven by the defects. Thus, higher sintering pressure could cause a higher degree of Cu NPs coalescence. For the impact brought by low sintering temperature, although it only played a role in promoting atomic diffusion, the effect varied with different microstructures of Cu NPs. If there were few defects generated during sintering, the coalescence of NPs occurred mainly via surface diffusion, which is slightly affected by elevated temperature. However, when extensive defects were generated during sintering, e.g. twin boundaries and dislocations, the atomic diffusion around defects started to play a dominant role in NPs coalescence, which can be significantly promoted by increasing temperature. In addition, the sintering pressure and temperature dependencies were also observed in the elastic modulus and tensile strength of the sintered Cu NPs. On one hand, the structure sintered under higher pressure and temperature resulted in better mechanical behavior, including a larger elastic modulus and tensile strength. On the other hand, in the temperature of 300 K to 500 K, the sintering pressure elevated from pressure-free condition to 300 MPa showed a significant

role in affecting the mechanical properties of Cu NPs, which is consistent with its effect on the coalescence degree of Cu NPs.

CRediT authorship contribution statement

Dong Hu: Conceptualization, Formal analysis, Investigation, Writing - original draft. **Zhen Cui:** Methodology, Software, Writing - review & editing. **Jiajie Fan:** Writing - review & editing, Supervision. **Xuejun Fan:** Writing - review & editing. **Guoqi Zhang:** Supervision, Project administration, Funding acquisition.

Declaration of Competing Interest

The authors declare that they have no known competing financial interests or personal relationships that could have appeared to influence the work reported in this paper.

Acknowledgements

This work was supported by the ECSEL Joint Undertaking (JU) under grant agreement No 826417. The JU receives support from the European Union's Horizon 2020 research and innovation programme and Germany, Austria, Spain, Finland, Hungary, Slovakia, Netherlands, Switzerland.

References

[1] Zhang GQ, Graef M, Van Roosmalen F. The rationale and paradigm of "More than Moore". Proc - Electron Components Technol Conf 2006;2006:151–7. https://doi.org/10.1109/ECTC.2006.1645639.
[2] Jones EA, Wang FF, Costinett D. Review of Commercial GaN Power Devices and GaN-Based Converter Design Challenges. IEEE J Emerg Sel Top Power Electron 2016;4:707–19. https://doi.org/10.1109/JESTPE.2016.2582685.
[3] Mantooth HA, Glover MD, Shepherd P. Wide Bandgap Technologies and Their Implications on Miniaturizing Power Electronic Systems. IEEE J Emerg Sel Top Power Electron 2014;2:374–85. https://doi.org/10.1109/JESTPE.2014.2313511.
[4] Chen Z, Guerrero JM, Blaabjerg F. A review of the state of the art of power electronics for wind turbines. IEEE Trans Power Electron 2009;24:1859–75. https://doi.org/10.1109/TPEL.2009.2017082.
[5] Hornbergers J, Lostetter AB, Mcnutt KIOT, Lal SM, Mantooth A. Silicon-Carbide (Sic) Semiconductor Power Electronics for Extreme High-Temperature Environments. 2004 IEEE Aerosp. Conf. Proc. (IEEE Cat. No.04TH8720) 2004: 2538–55.
[6] Khazaka R, Mendizabal L, Henry D, Hanna R. Survey of high-temperature reliability of power electronics packaging components. IEEE Trans Power Electron 2015;30:2456–64. https://doi.org/10.1109/TPEL.2014.2357836.
[7] Scheuermann U, Wiedl P. Low temperature joining technology - a high reliability alternative to solder contacts. Work. Met. Ceram. Mater. Funct. Appl. Vienna 1997: 181–92.
[8] Kim D, Nagao S, Chen C, Yamamoto Y, Wakasugi N, Kimoto Y, et al. GaN micro-heater chip for power cycling of die attach modules with Ag sinter joint and high temperature solder 2019:7–9.
[9] Zhao Y, Mumby-Croft P, Jones S, Dai A, Dou Z, Wang Y, et al. Silver sintering die attach process for IGBT power module production. Conf Proc - IEEE Appl Power Electron Conf Expo - APEC 2017:3091–4. https://doi.org/10.1109/APEC.2017.7931138.
[10] Siow KS, Chua ST, Beake BD, Zuruzi AS. Influence of sintering environment on silver sintered on copper substrate. J Mater Sci Mater Electron 2019;30:6212–23. https://doi.org/10.1007/s10854-019-00924-x.
[11] Zhang H, Minter J, Lee N. A Brief Review on High-Temperature, Pb-Free Die-Attach Materials. J Electron Mater 2019;48:201–10. https://doi.org/10.1007/s11664-018-6707-6.
[12] German R. Sintering: from empirical observations to scientific principles. Butterworth-Heinemann; 2014.
[13] Coblenz WS, Dynys JM, Cannon RMCR. Initial stage solid state sintering models. A critical analysis and assessment. Sinter Process Mater Sci Res 1980;13:141–57.
[14] Yadha V, Helble JJ. Modeling the coalescence of heterogenous amorphous particles. J Aerosol Sci 2004;35:665–81. https://doi.org/10.1016/j.jaerosci.2003.11.009.
[15] Djohari H, Derby JJ. Transport mechanisms and densification during sintering: II. Grain boundaries. Chem Eng Sci 2009;64:3810–6. https://doi.org/10.1016/j.ces.2009.05.022.
[16] Djohari H, Derby JJ. Transport mechanisms and densification during sintering: I. Viscous flow versus vacancy diffusion. Chem Eng Sci 2009;64:3799–809. https://doi.org/10.1016/j.ces.2009.05.022.
[17] Frenkel J. Viscous flow of crystalline bodies under the action of surface tension. J Phys (Moscow)1 1945;9:385–91.
[18] Pokluda O, Bellehumeur CT, Vlachopoulos J. Modification of Frenkel's model for sintering. AIChE J 1997;43:3253–6.
[19] Zhu H, Averback RS. Sintering processes of two nanoparticles: A study by molecular dynamics simulations. Philos Mag Lett 1996;73:27–33. https://doi.org/10.1080/095008396181073.
[20] Cheng B, Ngan AHW. The crystal structures of sintered copper nanoparticles: A molecular dynamics study. Int J Plast 2013;47:65–79. https://doi.org/10.1016/j.ijplas.2013.01.006.
[21] Lange AP, Samanta A, Majidi H, Mahajan S, Ging J, Olson TY, et al. Dislocation mediated alignment during metal nanoparticle coalescence. Acta Mater 2016;120: 364–78. https://doi.org/10.1016/j.actamat.2016.08.061.
[22] Zhang Y, Wu L, El-Mounayri H, Brand K, Zhang J. Molecular Dynamics Study of the Strength of Laser Sintered Iron Nanoparticles. Procedia Manuf 2015;1:296–307. https://doi.org/10.1016/j.promfg.2015.09.031.
[23] Grammatikopoulos P, Cassidy C, Singh V, Benelmekki M, Sowwan M. Coalescence behaviour of amorphous and crystalline tantalum nanoparticles : a molecular dynamics study. J Mater Sci 2014;49:3890–7. https://doi.org/10.1007/s10853-013-7893-5.
[24] Goudeli E, Pratsinis SE. Crystallinity Dynamics of Gold Nanoparticles During Sintering or Coalescence. AIChE J 2016;62:589–98. https://doi.org/10.1002/aic.
[25] Ding L, Davidchack RL, Pan J. A molecular dynamics study of sintering between nanoparticles. Comput Mater Sci 2009;45:247–56. https://doi.org/10.1016/j.commatsci.2008.09.021.
[26] Grammatikopoulos P, Sowwan M, Kioseoglou J. Computational Modeling of Nanoparticle Coalescence. Adv Theory Simulations 2019;2:1900013. https://doi.org/10.1002/adts.201900013.
[27] Knoerr M, Kraft S, Schletz A. Reliability assessment of sintered nano-silver die attachment for power semiconductors. 2010 12th Electron. Packag. Technol. Conf. EPTC 2010, IEEE; 2010, p. 56–61. 10.1109/EPTC.2010.5702605.
[28] Zhao SY, Li X, Mei YH, Lu GQ. Study on high temperature bonding reliability of sintered nano-silver joint on bare copper plate. Microelectron Reliab 2015;55: 2524–31. https://doi.org/10.1016/j.microrel.2015.10.017.
[29] Srivastava I, Peters BL, Lane JMD, Fan H, Salerno KM, Grest GS. Mechanics of Gold Nanoparticle Superlattices at High Hydrostatic Pressures. J Phys Chem C 2019;123: 17530–8. https://doi.org/10.1021/acs.jpcc.9b02438.
[30] Cheng B, Ngan AHW. The sintering and densification behaviour of many copper nanoparticles: A molecular dynamics study. Comput Mater Sci 2013;74:1–11. https://doi.org/10.1016/j.commatsci.2013.03.014.
[31] Yang S, Kim W, Cho M. Molecular dynamics study on the coalescence kinetics and mechanical behavior of nanoporous structure formed by thermal sintering of Cu nanoparticles. Int J Eng Sci 2018;123:1–19. https://doi.org/10.1016/j.ijengsci.2017.11.008.
[32] Zhang Y, Zhang J. Sintering phenomena and mechanical strength of nickel based materials in direct metal laser sintering process - A molecular dynamics study. J Mater Res 2016;31:2233–43. https://doi.org/10.1557/jmr.2016.230.
[33] Wang F, Tang Z, He H. Stress-dislocation interaction mechanism in low-temperature thermo-compression sintering of Ag NPs. AIP Adv 2018;8. https://doi.org/10.1063/1.5024593.
[34] Plimpton S. Fast parallel algorithms for short-range molecular dynamics. J Comput Phys 1995;117:1–19. https://doi.org/10.1006/jcph.1995.1039.
[35] Adams JB, Foiles SM, Wolfer WG. Self-diffusion and impurity diffusion of fcc metals using the five-frequency model and the Embedded Atom Method. J Mater Res 1989;4:102–12. https://doi.org/10.1557/JMR.1989.0102.
[36] Wang L, Guan P, Teng J, Liu P, Chen D, Xie W, et al. New twinning route in face-centered cubic nanocrystalline metals. Nat Commun 2017;8:1–7. https://doi.org/10.1038/s41467-017-02393-4.
[37] Wolf D, Yamakov V, Phillpot SR, Mukherjee A, Gleiter H. Deformation of nanocrystalline materials by molecular-dynamics simulation: Relationship to experiments? Acta Mater 2005;53:1–40. https://doi.org/10.1016/j.actamat.2004.08.045.
[38] Grammatikopoulos P. Atomistic modeling of the nucleation and growth of pure and hybrid nanoparticles by cluster beam deposition. Curr Opin Chem Eng 2019;23: 164–73. https://doi.org/10.1016/j.coche.2019.04.004.
[39] Samsonov VM, Talyzin IV, Vasilyev SA, Alymov MI. Mechanisms of Coalescence of Metallic Nanodroplets and Sintering of Metallic Nanoparticles. Dokl Phys 2019;64: 453–5. https://doi.org/10.1134/S1028335819120061.
[40] Stukowski A. Visualization and analysis of atomistic simulation data with OVITO – the Open Visualization Tool. Model Simul Mater Sci Eng 2010;18:015012. https://doi.org/10.1088/0965-0393/18/1/015012.
[41] Dong HAI, Moon K, Wong CP. Molecular Dynamics Study on the Coalescence of Cu Nanoparticles and Their Deposition on the Cu Substrate. J Electron Mater 2004;33: 1–5.
[42] Li Q, Wang M, Liang Y, Lin L, Fu T, Wei P, et al. Molecular dynamics simulations of aggregation of copper nanoparticles with di ff erent heating rates. Phys E Low-Dimensional Syst Nanostructures 2017;90:137–42. https://doi.org/10.1016/j.physe.2017.03.024.
[43] Goudeli E, Pratsinis SE. Surface Composition and Crystallinity of Coalescing Silver−Gold Nanoparticles. ACS Nano 2017;11:11653–60. https://doi.org/10.1021/acsnano.7b06727.
[44] Arcidiacono S, Bieri NR, Poulikakos D, Grigoropoulos CP. On the coalescence of gold nanoparticles. Int J Multiph Flow 2004;30:979–94. https://doi.org/10.1016/j.ijmultiphaseflow.2004.03.006.
[45] Surblys D, Matsubara H, Kikugawa G, Ohara T. Application of atomic stress to compute heat flux via molecular dynamics for systems with many-body interactions. Phys Rev E 2020;99:051301. https://doi.org/10.1103/PhysRevE.99.051301.

[46] Youssef K, Sakaliyska M, Bahmanpour H, Scattergood R, Koch C. Effect of stacking fault energy on mechanical behavior of bulk nanocrystalline Cu and Cu alloys. Acta Mater 2011;59:5758–64. https://doi.org/10.1016/j.actamat.2011.05.052.
[47] Stukowski A, Bulatov VV, Arsenlis A. Automated identification and indexing of dislocations in crystal interfaces. Model Simul Mater Sci Eng 2012;20:1–16. https://doi.org/10.1088/0965-0393/20/8/085007.
[48] Faken D, Jonsson H. Systematic analysis of local atomic structure combined with 3D computer graphics. Comput Mater Sci 1994;2:279–86.
[49] Li J, Shi T, Yu X, Cheng C, Fan J, Liao G, et al. IEEE 67th Electron. Components Technol. Conf. 2017;2017:976–81.
[50] Liu J, Chen H, Ji H, Li M. Highly Conductive Cu-Cu Joint Formation by Low-Temperature Sintering of Formic Acid-Treated Cu Nanoparticles. ACS Appl Mater Interfaces 2016;8:33289–98. https://doi.org/10.1021/acsami.6b10280.
[51] Mou Y, Peng Y, Zhang Y, Cheng H, Chen M. Cu-Cu bonding enhancement at low temperature by using carboxylic acid surface-modified Cu nanoparticles. Mater Lett 2018;227:179–83. https://doi.org/10.1016/j.matlet.2018.05.037.
[52] Meng L, Zhang Y, Yang X, Zhang J. Atomistic modeling of resistivity evolution of copper nanoparticle in intense pulsed light sintering process. Phys B Condens Matter 2019;554:31–4. https://doi.org/10.1016/j.physb.2018.11.036.
[53] Ishizaki T, Miura D, Kuno A, Hasegawa K, Usui M, Yamada Y. Young's modulus of a sintered Cu joint and its influence on thermal stress. Microelectron Reliab 2017; 76–77:405–8. https://doi.org/10.1016/j.microrel.2017.06.015.